Experimental and numerical investigation of CO_2 laser ablation of fused silica with sub-microsecond pulses

C. Cifuentes Quintal,[1] P. Cormont,[2] and L. Gallais[1, a)]

[1)] *Aix Marseille Univ, CNRS, Centrale Marseille, Institut Fresnel, Marseille, France*

[2)] *CEA-CESTA, 15 Avenue des Sablières, CS 60001, F33116 Le Barp Cedex, France*

(Dated: 5 August 2021)

The CO_2 laser-material interaction is commonly used for thermal treatments and processing of fused silica glasses. As the laser pulse duration decreases down to few tens of microseconds the heat affected depth in the material decreases up to the point where it has the same magnitude as the laser radiation penetration depth, which is an interesting operating point for applications that require minimal heat affected zone. In this work we explore the effects of CO_2 laser pulses in the range of 100 μs to few ms on the laser ablation of polished fused silica surfaces, based on experiments and numerical simulations. We particularly study the evolution of surface profile as a function of the number of applied pulses. The results suggest that the ablation depth can be accurately controlled from few hundreds of nanometers to few tens of micrometers by adjusting the combination of the number of applied pulses and pulse duration.

[a)] laurent.gallais@fresnel.fr

I. INTRODUCTION

CO_2 laser processing of glass has been used for decades, but it is still a very active field of research to develop innovative processes. Recent interests include for instance optics manufacturing[1–4], surface micromachining[5–8], to produce refractive or diffractive optical elements, processing of optical fibers[9–13], including end-facet, fiber or cladding processing, or mitigation of surface damage in high power laser components[14–18], such as laser damage or scratches. The CO_2 laser-material interaction is particularly suitable for thermal treatments and processing of fused silica because this glass has a high thermal shock resistance due to a low thermal expansion coefficient[19]. Microcracking can be observed on other common types of glasses, such as borosilicate, because of residual thermo-mechanical stress[19,20]. The physical process of the laser glass interaction involves absorption of the laser radiation in the skin layer, temperature rise with strong modifications of material viscosity associated to viscous and capillary mass transport, and evaporation if sufficient laser energy is deposited. Then during the cooling phase subsequent to laser heating, changes of the glass properties compared to its initial state occur in the heat affected area (described as changes of the fictive temperature) associated to thermo-mechanical stresses. These physical processes lead to structural changes in the material such as densification, birefringence, surface smoothing, and crater formation. Understanding these processes and evaluating their effects depending on the laser irradiation conditions is of paramount importance to support the application developments. In such efforts, one of the main difficulty is to accurately describe the behavior of fused silica at high temperature, up to 3000 K.

In this context there have been several developments of models to describe these physical effects in the operating range of CO_2 lasers (pulse irradiation from μs to seconds) in order to identify suitable process parameters. Feit et al[21] took into account laser energy absorption, heat conduction and radiation to obtain estimates and order of magnitude of material removal by evaporation and thermally induced stresses. Nowak et al[22] have described a 1D analytical model of CO_2 laser ablation of fused silica based on thermodynamical consideration and a defined temperature threshold (boiling temperature, 3085 K) for the onset of ablation. This model describes accuratelly the reported data by the authors (ablation threshold and removal rate) in the explored pulse duration range (10-100 μs) supporting the hypotehsis that material removal can be described as a non explosive process

in such conditions. These models provide insights into the physical mechanisms and first order estimates but they have limitations to tackle the strong non-linearities at high temperature, complex geometries (with moving laser beam for instance) and strong interplay between the different physical processes. Numerical models based on multiphysics finite-element methods can provide such descriptions of the interactions but they need accurate material descriptions, validated by experiments. With such approaches Vignes et al[23] have worked on thermomechanical modeling of laser-induced structural relaxation and deformation of fused silica heated at high temperatures. Their model is able to describe nanometric surface profile changes related to structural modifications (densification) and the development of residual stresses, with excellent agreement between experiment and simulations in the long pulse regime (seconds). We have also detailed the development of comprehensive thermo-mechanical numerical simulations of these physical processes, based on finite-element method[24], with choice of the different inputs parameters based on dedicated experiments: infrared thermography, optical profilometry, furnace annealing, photo-elastimetry or wavefront propagation measurements[25–27]. In the continuation of this work, we present in this paper our last progress in the improvement of the description of the laser material interactions under consideration. We particularly focus on the silica surface modifications (evaporation, densification) in the perspective of obtaining a model which we can rely on to describe these modifications in the range of CO_2 laser operating conditions that can be used for microprocessing with pulsed ablation (from microsconds to milliseconds).

This paper is presented in 3 parts. In section II we detail the model used in this work. This includes a short description of the thermo-mechanical model that has been published in Ref 24 which is the basis of our present work, followed by our recent developments to describe silica modifications after pulsed laser irradiation. Then in section III we report on experiments conducted on fused silica samples with pulsed CO_2 irradiations in the range from 100 microseconds to few milliseconds. We particularly study the evolution of surface profile as a function of the number of applied pulses. Then in section IV we compare experimental results to simulations, and discuss the applicability and limits of the numerical model.

II. MODEL

A. Heat source and heat equation

The starting point of the work is based on Ref 24. Therefore it is of importance to recall the approach, the main assumptions and the materials properties we use.

The laser source is described as an arbitrary intensity distribution at the surface, that will be described as a Gaussian distribution on the surface in the present study. The intensity distribution along the propagation direction in the skin layer of the material is solved numerically, considering the dependence of the complex refractive index with temperature based on reported data by McLachlan and Meyer[28]. Such approach allows to take into account for the changes of the extinction coefficient within the depth of the heated material. Variations of reflectivity with temperature are also considered.

Based on the volume heat source induced by laser absorption, we solve the heat equation considering heat transfer by conduction in the material, and radiation losses at the surface. Thermal properties and their temperature dependence are based on the work of Combis et al[29].

B. Heat affected zone

Laser processing of glass can impose very fast heating and cooling rates that affect the glass structure in the heat affected zone. During the cooling phase, the glass network undergoes structural changes that depends on the cooling rate up to the point where it frozens because of the strong increase of viscosity with the temperature decrease. Therefore the laser-processed glass can exhibit different properties from those of the original material, such as a change of density. In borosilicate glasses the rapid cooling down subsequent to laser heating leads to a decrease of the glass density[30]. This rapid cooling results in an increase of the glass volume in the heat affected area and surface deformations on the glass surface in the form of bumps[6,30,31]. However the fused silica glasses exhibit the opposite effect: an increase of the glass density leading to surface deformation in the form of depressions within the laser-irradiated area[6,26]. In order to estimate these modifications we have implemented in the numerical model the calculation of fictive temperature (T_f), which characterizes the structural state of the glass. The fictive temperature of the glass reflects the temperature

at which the liquid structure is frozen into the glassy state during the cooling phase. The variation of fictive temperature with time can be calculated as:

$$\frac{dT_f}{dt} = \frac{T - T_f}{\tau(T, T_f)} \tag{1}$$

where T is the thermodynamic temperature and τ is the relaxation time, that is function of the fictive and thermodynamic temperature. High purity silica glass exhibits an exponential structural relaxation time[32] that can be described with the following expression:

$$ln(\tau) = ln(\tau_0) + [\frac{Q_1}{RT} + \frac{Q_2}{RT_f}] \tag{2}$$

where τ_0 is the relaxation time at T and T_f=$+\infty$, and Q_1 and Q_2 are activation energies. These activations energies can be described as a partition of the activation enthalpy, ΔH, between thermodynamic and fictive temperature contribution: $Q_1 = x\Delta H$ and $Q_2 = (1 - x)\Delta H$. In fused silica however the relaxation time has little dependence on T_f[32]. Vignes et al[23] estimated x=0.9 in conditions of CO_2 laser heating. In our previous work[33] we have estimated a value of ΔH=457 kJ/mol, with x= 1 obtained from fitting experimental data.

We have plotted on Fig. 1 the fictive temperature distributions obtained in the case of different laser pulse irradiations, from 100 μs to 100 ms. The power has been adjusted for each pulse duration so that the same surface temperature is reached at the end on the irradiation: 2800 K, which is close to the onset of vaporization of the material[14,22].

As the pulse duration decreases, the heat affected depth decreases up to the point where it is confined to the optical penetration depth of the laser radiation: as shown on Fig. 1-d, the material is modified (fictive temperature change) for 100 μs pulse in a depth of 9 μm below the surface, which is less than the laser wavelength. The minimal heat affected depth is reached with pulses of 100 μs. For long pulses up to seconds, it can reach almost one hundred microns. If the depth of the heat affected zone can be understood based on heat conduction considerations, the dependence of final fictive temperature with pulse duration is more complex to analyze: the fictive temperature increases from 1700 K for 1 s pulse irradiation to 1950 K for 100 μs pulse. The cooling dynamic must be taken into consideration to understand these differences. We have for instance plotted on Fig. 2 the evolution of temperature during the cooling phase for different pulse durations, and compared it to the relaxation time, as defined in Equation 2. The intersection of the different thermodynamic paths plotted on this figure with the relaxation time plot corresponds approximately to the

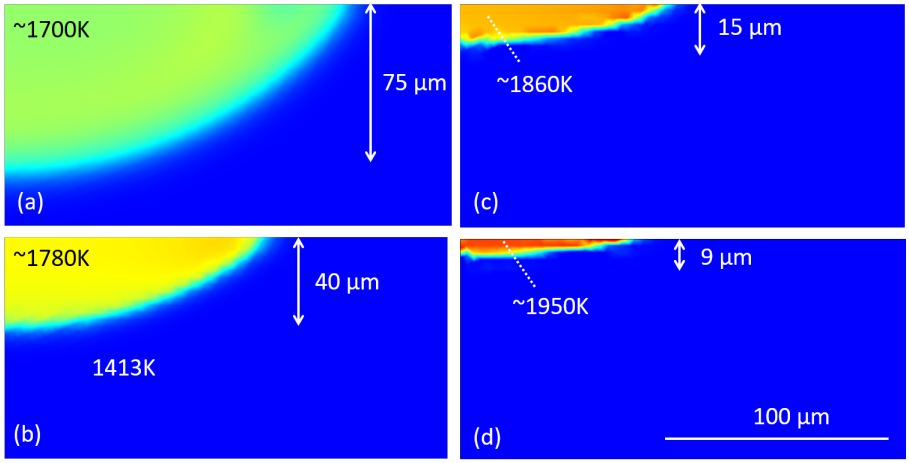

FIG. 1. 2D maps of the fictive temperature obtained after different CO_2 laser irradiations on fused silica with a spot size of 400 μm and (a) 100 ms / 4.05 W ; (b) 10 ms / 5.80 W ; (c) 1 ms / 14W ; (d) 0.1 ms / 55W. These parameters have been set to reach 2800 K at the surface.

point where the fictive temperature should "froze". A clear view of the relation between cooling rate after laser heating and the resulting fictive temperatures can be obtained with this plot. Short pulses will lead to relatively high fictive temperature compared to the initial glass (1413 K in our simulations), with some consequences in terms of surface modification.

C. Densification

As shown previously, depending on the laser irradiation conditions the heat affected zone can have different characteristics in terms of expanse and fictive temperature. The changes of glass microstructure, reflected by the fictive temperature, result in density changes near the glass surface. In the case of fused silica glass the density has a linear and positive relationship with the fictive temperature[34]. The consequence of this increase of density with the fictive temperature is a shrinking of the glass volume in the heat-affected area and the creation of deformation of the surface profile in the form of depressions[35]. With the knowledge of the fictive temperature distribution it is possible to obtain the density distribution in the material using the density dependence reported by Shelby[34]. The surface profile modification can then be obtained by integrating the density modifications along the the sample thickness. This simulation has been done for the different cases shown on Fig. 1 and is reported on Fig. 3.

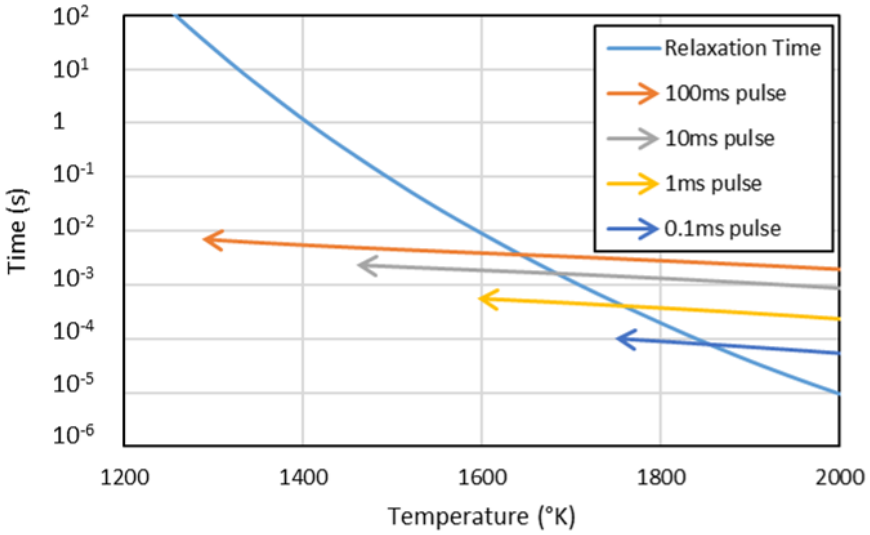

FIG. 2. Plots of the relaxation time as a function of temperature (in blue) and thermodynamic paths during cooling after heating with different pulse durations (other colors). The paths are calculated at the surface and at the center of the laser-heated area, with $t = 0$ the end of laser pulse.

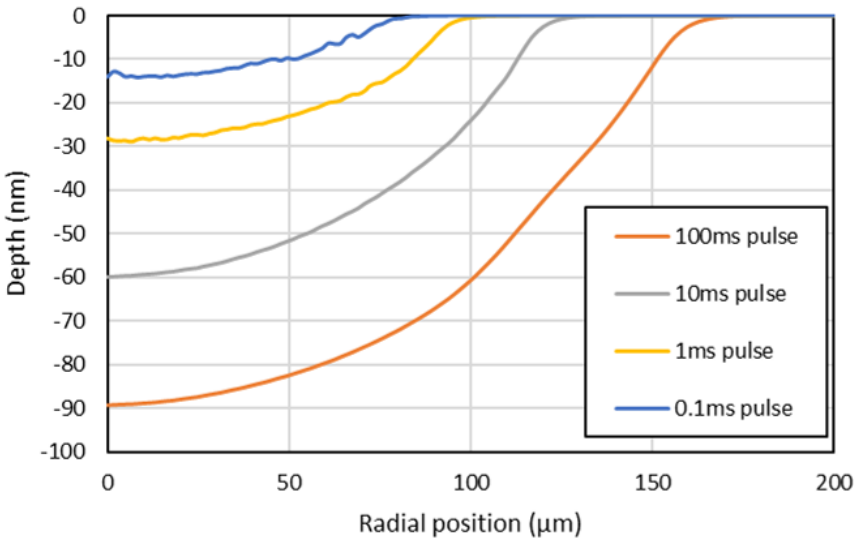

FIG. 3. Surface profiles obtained by taking into account densification of the heat affected area for different irradiation conditions (corresponding to the cases of Figure 1).

Surface profile modifications related to densification, and in conditions where no other mechanism occur such as evaporation, lie in the range from few nm up to 100 nm, depending on the pulse duration. This corresponds to experimental observations in reported works on

this topic: for instance 10 nm for 40 μs in Ref.[36], and 60 nm for few seconds in Ref.[35] .

D. Evaporation

Different works have investigated the formation of craters due to evaporation of silica in the case of CO_2 laser process. Based on data on the variation of silica vapor pressure as a function of temperature, Mendez et al.[37] have estimated that substantial ablation of silica must be expected at temperature above 2900-3000 K, corresponding to the range where the vapor pressure exceeds the atmospheric pressure. In a following work the same group has proposed an analytical model[22] to describe CO_2 laser-controlled ablation of fused silica, based on a sharply defined temperature threshold for material removal, practically equal to the boiling temperature of silica glass (3085 K). However this applies for short laser pulses ($< 100\mu s$) and other works indicate significant mass losses by evaporation in case of long pulses ($< 1s$) for temperatures as low as 2100 K[38].

As a first approach it is possible to evaluate the rate of material evaporation based on thermodynamics and kinetic theory of gases. The mass loss dm per unit of time dt and surface area dS and at temperature T can be expressed as[39]:

$$\frac{dm}{dtdS} = P_{sat}\sqrt{\frac{M}{2\pi RT}} \tag{3}$$

with M being the molar mass of silica, R the perfect gas constant, and p_{sat} the saturating vapor pressure. This last parameter is obtained under conditions of perfect gas assumption, ignoring vapor re-deposition, radial gradient effects and the formation of different silicon oxide species, but it should give an upper limit on the ejection rate. p_{sat} can be expressed with the Clausius-Clapeyron equation:

$$P_{sat} = P_0 exp\left(\frac{\Delta H_v}{R}\left(\frac{1}{T_b} - \frac{1}{T}\right)\right) \tag{4}$$

where T_b is the boiling temperature at pressure P_0 and ΔH_v the enthalpy of vaporization. The reported boiling temperature of silica is spread over a considerable range between 2500 K and 3300 K[40]. We used $T_b = 3085\,K$ which is a recommended value in Ref[40]. From Equation 3, the velocity of the evaporation front at the surface is given by:

$$v(T) = \frac{P_{sat}(T)}{\rho(T)}\sqrt{\frac{M}{2\pi RT}} \tag{5}$$

with $\rho(T)$ the density of the liquid phase. This theoretical velocity, which should be considered as a theoretical maximum limit, is plotted on Figure 4. As shown in the study dedicated to the evaporation kinetics of fused silica at high temperature by Elhadj et al[41], the rates predicted by this theoretical approach derived from the kinetic theory of gases can be 2 to 3 orders of magnitude greater than the measured evaporation rates. The rate is reduced because of mass transport limitation in the conditions of laser-based evaporation. By introducing in the right hand side of Eq. 5 a coefficient β (which is smaller than unity), we can empirically take into account the various factors lowering the evaporation rate and define an effective evaporation rate:

$$v_{eff}(T) = \beta v(T) \tag{6}$$

This coefficient β will be discussed later in the discussion section.

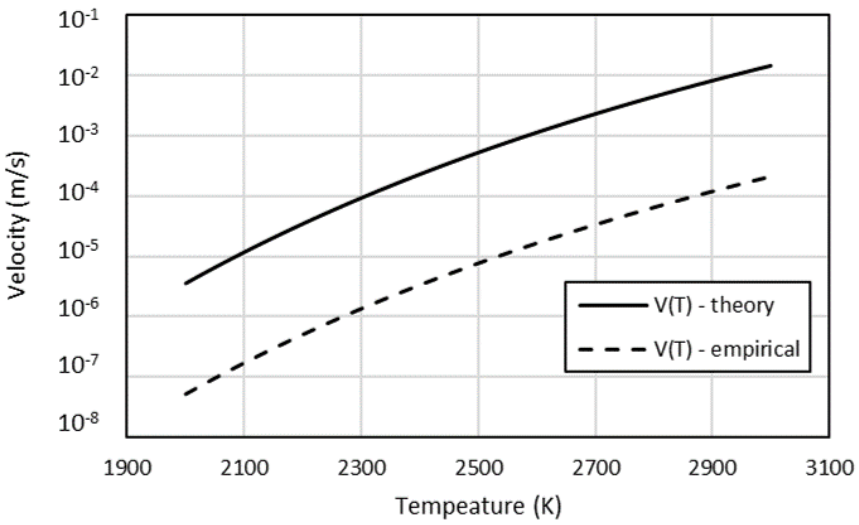

FIG. 4. Velocity of the evaporation front as a function of temperature. Plain line curve corresponds to the theoretial velocity calculated from the kinetic theory of gas. Dash line curve corresponds to the velocity determined from experiments (effective velocity) with the application of β coefficient.

In order to investigate the crater formation dynamic by evaporation, we have a used a moving mesh method in the numerical simulation, with a surface recession velocity determined by Eq. 6. We however neglect at this step the effects of the vapor on the laser beam propagation.

Evaporative cooling has also to be considered in our conditions, particularly for the case

when craters deeper than the laser penetration depth are created. It was taken into account in our simulations as an outgoing heat flux given by the expression:

$$\Phi_{out} = v_{eff}(T)\rho(T)\frac{U}{M} \tag{7}$$

Eventually the model is described in the schematic of Figure 5 to summarize the simulation conditions.

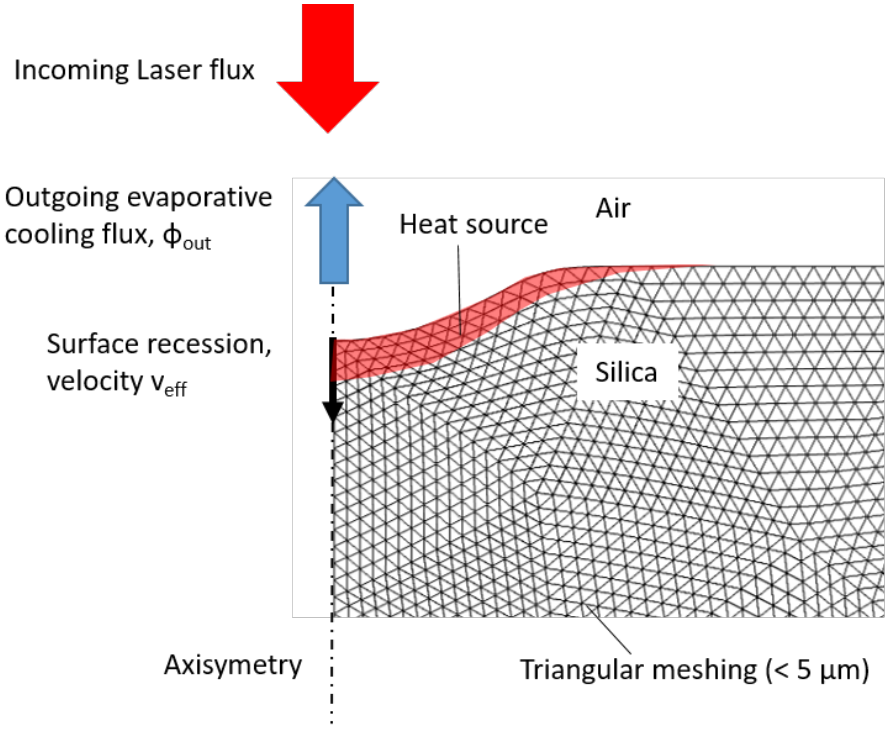

FIG. 5. Schematic of the simulation conditions.

III. EXPERIMENTS

A. Experimental system

The experimental system that has been used in this work has been described in details in Ref.[16]. We will only briefly indicate the main specifications of interest for the present work.

The source is a radio frequency excited CO_2 laser (Rofin SR10i, UK) operating at 10.6-μm wavelength. The wavelength was not measured and according to the manufacturer specification it may vary from 10.45 to 10.7 μm. This variation was not taken ino account in our simulations. A maximum output power of 120 W is delivered with an active power

feedback system to reach a stability of 2% peak to peak and of 0.5% standard deviation. In our experiments, the laser was used at its maximum modulation rate (130 kHz) and duty cycle (60%), to reach a quasi-CW output. The laser beam delivered to the sample was provided by the first diffraction order beam generated by a germanium crystal acousto-optic modulator (AOM). The AOM allows an accurate control of the laser power and pulse duration. This beam was directed on the sample through a 200 mm focal length plano-convex ZnSe lens. The beam is Gaussian in the focal plane, with an ellipticity < 0.95. The beam radius at $1/e^2$ is $w_{1/e^2} = 266\mu m \pm 10\%$ with a corresponding radius at $1/e$ $w_{1/e} = 188\mu m \pm 10\%$ (measured with the knife-edge method). Taking into account the different losses in the beam transport and delivery, 85 W are available on the sample plane and all the experiments were done at this maximal power. Only the pulse duration was modified in our study: we have worked with pulses from $100\mu s$, minimum pulse duration to obtain modification of the surface in our conditions, to few ms. This pulse duration was set with a digital delay generator (DG 535, Standford Research Instrument) used as the gate input of the AOM.

B. Samples and test procedures

The samples under study are made of fused silica (C7980, Corning) and are polished. They have diameter of 50 mm and a thickness of 5 mm.

We will report particularly on the results obtained on two set of experiments. For the first one we were interested in carrying out a statistical study of the crater profiles, so we have shot the laser at a given power and pulse duration on each location just one time. We varied the duration of shots from 100 μs to 1 ms to obtain 20 craters at the same irradiation time and then compared their variations. For the second experiment, we were interested in studying the evolution of crater profile depending on the number of shots, so this time we shot several times at the same site, from 1 to 16 shots, with pulse durations ranging also from 100 μs to 1 ms.

C. Measurements of crater profiles

We have used an optical profilometer based on coherence correlation interferometry (Newview 7300, Zygo) to measure the surface topography of the irradiated sites. Optical profiles of each irradiated site was measured with a 10X objective and a numerical aperture of 0.30, which allows a measurement area of 700 μm x 530 μm with an optical resolution of 0.95 μm. Step height standards provided by the manufacturer were used to calibrate the measurement. In Fig. 6 (a) we show one example of measurement on a shallow crater. For deep craters such as those created with irradiation time longer than 500 μs in our conditions, it is not possible to reconstruct the complete profile because of the steep slope of the crater. In these case, only a partial measurement of the profile is obtained (surface of the sample and bottom of the crater, see for instance Figure 6 (b)). Nevertheless this measurement is sufficient to obtain the depth of the crater.

D. Experimental Results

We have conducted a parametric study on 2 parameters: the effect of pulse duration and the effect of the number of shots on the crater morphology. The other experimental parameters, the beam size and the power, were kept unchanged.

1. Pulse duration

In our experimental conditions, the onset of surface modification corresponds to pulse durations of approximately 100 μs, therefore we have not been able to explore effects at shorter pulse durations. In accordance to our study objectives which were to identify best conditions to ablate silica while minimizing the heat affected area, we have restricted our study to 1 ms as the longer pulse duration, thus exploring one decade of irradiation time. We report on Figure 7 on the evolution of the crater depth with the irradiation time, taking into account the statistical variations obtained on 30 different sites per condition. The crater morphologies and their comparison with simulations will be discussed in the next section.

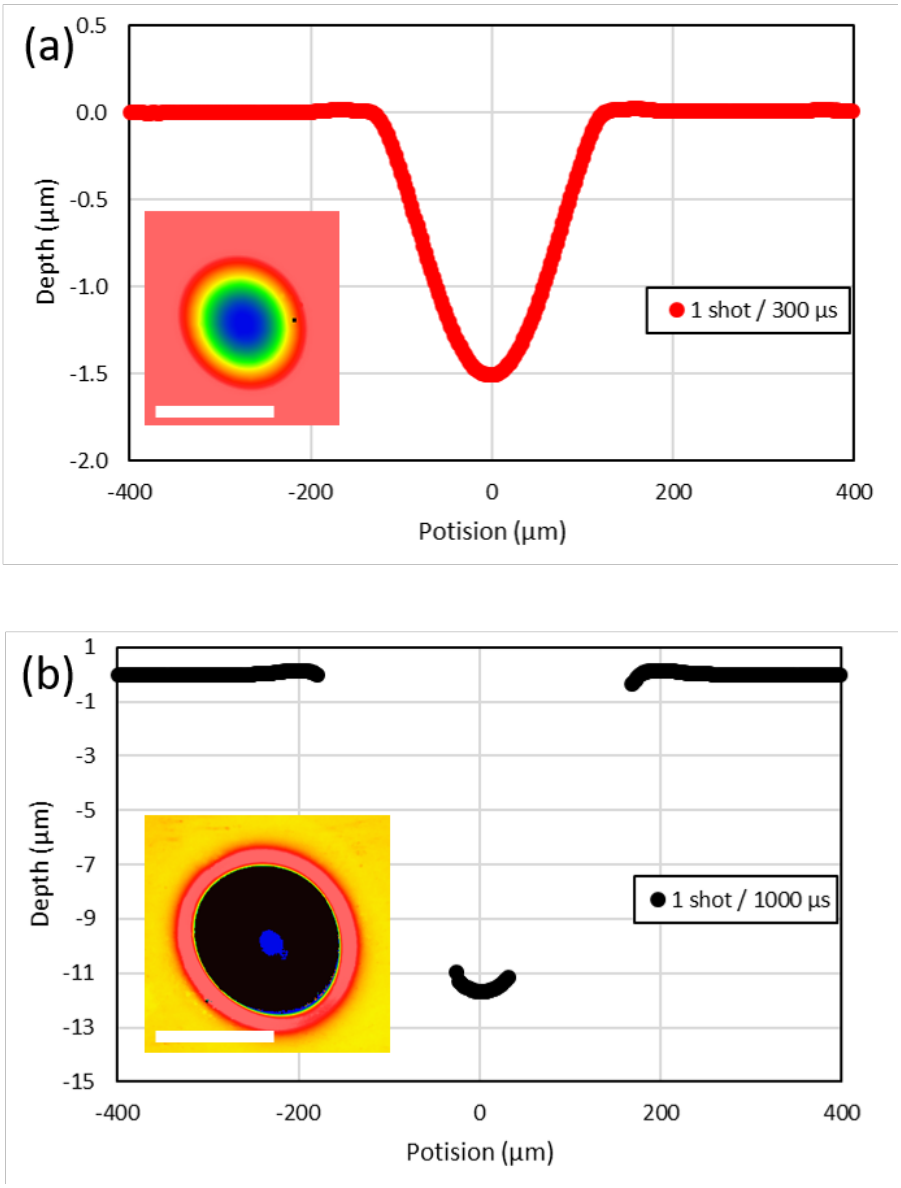

FIG. 6. Surface profiles measured with optical profilometer. The inserted images show the surface topograhy with a scale bar of 200 μm. Irradiation conditions (a) 300 μs, 85W ; (b) 1000 μs, 85W.

2. Pulse repetition

We have investigated the effect of the number of applied pulses on the crater morphology, with a number of pulses from 1 to 16. In these experiments, a delay of 1 s has been set between each pulse in order for the material to cool down before the next irradiation. The results are plotted on Figure 8 for different pulse durations. The data is given on different graphs for clarity. The profiles of these different craters are shown and discussed in the next

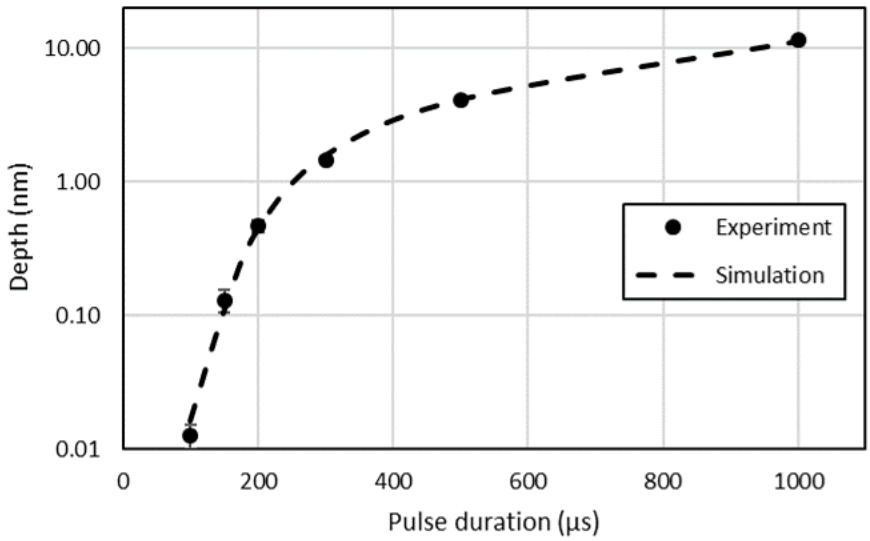

FIG. 7. Evolution of the depth of the craters with the pulse duration. The experimental data corresponds to a mean value on 30 sites, with the error bars given as plus/minus the standard deviation. The dashed line corresponds to the numerical simulations.

section, by comparing them to the numerical simulations.

For low pulse duration, $100\,\mu s$, the surface modification of few ten of nm corresponds to a regime of densification and a linear evolution can be observed. A linear regression can also be applied to the data obtained for pulses longer than $200\,\mu s$, a regime that corresponds to material evaporation with material removal. Interestingly, we do not observe any saturation as the number of pulses increases. The pulse duration of $150\,\mu s$ should correspond to an intermediate state between these two effects and a linear evolution is not observed. These results suggest that the ablation depth in laser processing applications can be accurately controlled in a large range of depth by the number of applied pulses and pulse duration. However if the linear evolution is understandable in an ablation regime controlled by evaporation (the same material quantity is evaporated at each shot) it is more difficult to understand in the regime of densification since this regime is controlled by the heat affected zone, that should be the same for each shot. This will be discussed in the next section.

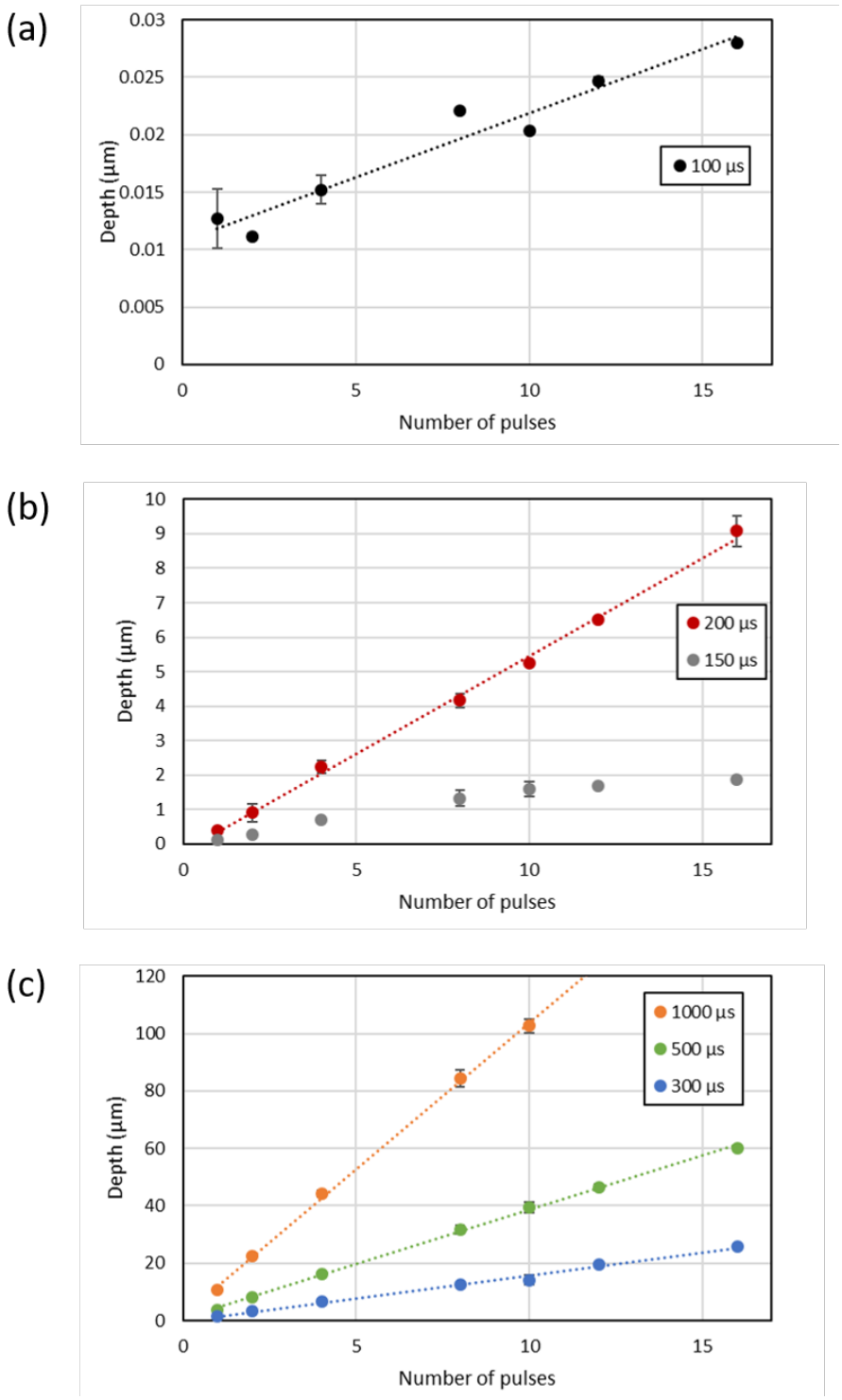

FIG. 8. Evolution of the depth of the craters with the number of pulses for different pulse durations. (a) Case of 100 μs pulses ; (b) 150 and 200 μs ; (c) 300, 500 and 1000 μs. The dashed line corresponds to a linear fit of the data (in the case of pulses of 150 μs the evolution was non linear).

IV. DISCUSSION

We now proceed to discuss on the comparison of experimental and numerical results, in a first part for the case of single shot irradiation and in a second part for the case of multiple shots on the same location.

A. Evolution of crater profiles with pulse duration

Experimental results have shown that in our experimental conditions, the crater depth is below 100 nm for pulse durations shorter than 100 μs (see Figure 7). Profilometry measurements of the crater profiles reveal that a transition occurs between 100 μs and 150 μs (Figure 7) which could be considered as the onset of material evaporation. The observed craters below 100 μs are in this case related to surface modification by densification. The comparison of simulated crater profile to the experimental one is shown on Figure 9 (a) for 100 μs irradiation time. In the simulations the onset of evaporation is not reached and the surface modification is caused only by density change and material contraction. Even if the calculated shape does not corresponds perfectly to the measured one, particularly considering the large diameter of the experimental crater, the depth are in close agreement. The relatively large diameter of the experimental crater is still unclear and cannot be explained on the basis of fictive temperature change in our model since the experimental crater extends out of the heated area. One possible cause of discrepancy between simulation and experiment could be that the spatial shape of the beam is not perfectly gaussian. The beam shape being measured with the knife-edge method and not directly with an imaging system, it is difficult to go further on this point. For longer durations, greater that 150 μs, the material is removed by evaporation according to the simulation. In that case the model can match very well the measured crater profiles, for $\beta = 0.015$, as shown on figure 9 (b) to (c). For craters as deep as 10 μm, obtained for 1 ms pulse irradiation, an excellent agreement is obtained on the evolution of crater depth with exposure time (Figure 7). Such value of β is consistent with the work of Elhadj et al[41] that demonstrate very low evaporation rates of silica in air, compared to the ones predicted by equation 3. We can note the different shapes between crater related to densification (figure 9 (a)) or evaporation (figure 9 (c), (d)), the case shown in figure 9 (b)) being an intermediate between both since it corresponds to the

onset of evaporation.

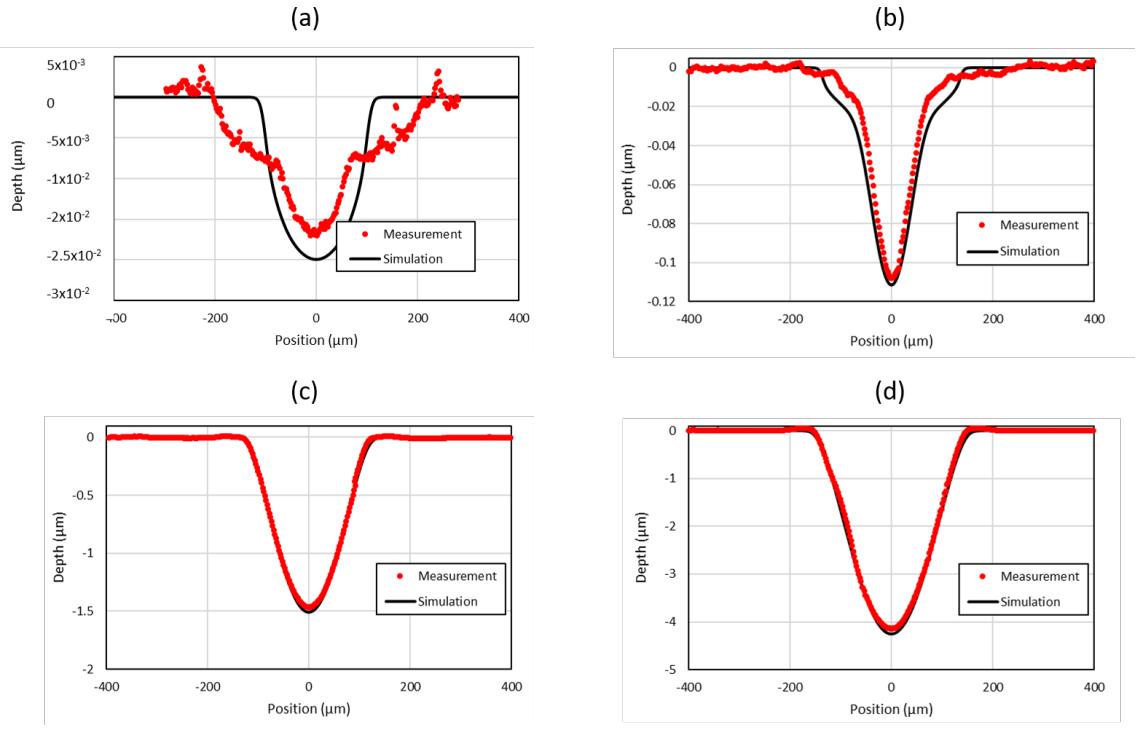

FIG. 9. Measured crater profiles and comparison to simulations. Case a single irradiation with (a) 100 μs, (b) 150 μs, (c) 300 μs, (d) 500 μs.

B. Effect of the number of applied pulses

As discussed previously the numerical model can accurately describe the evolution of crater shape with the laser processing parameters. In the case of multiple irradiations it has been observed that the crater depth evolves linearly with the number of applied pulses (Figure 8). This means that the laser irradiation has the same effect on the material in case of pristine surface or a crater, which indicates that the absorption does not depend on the crater shape and potential modified material properties in the crater. We have conducted numerical simulations corresponding to this case using the crater profile after one shot as an input for the next shot. Not surprisingly the crater profile is also well described by the numerical model, as shown for one example on Figure 10, since we use the same absorption and material properties during the sequences. This excellent agreement has been obtained for pulse duration from 200 μs to 1000 μs, but not for shorter pulse durations where densification

is the main mechanism of crater formation. In that case the model cannot describe any evolution with the number of pulses: the same temperature gradient is reproduced for each shot therefore there cannot be any further fictive temperature modification after the first shot. A possible explanation of the observed experimental behaviour in case of short pulse durations could be a slight participation of evaporation.

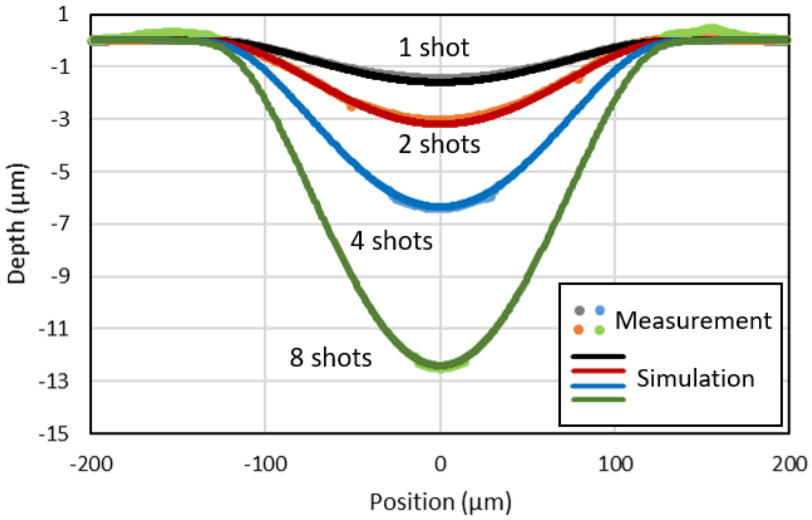

FIG. 10. Measured crater profiles and comparison to simulations. Case of successive irradiations on the same site.

V. CONCLUSION

The objective of our work was to obtain a better understanding of surface profile modifications corresponding to laser material interaction in a regime that is particularly interesting for processing silica optical components. A numerical model was able to provide an excellent description of the crater morphology as a function of laser parameters (which are mainly power, beam size, pulse duration and the number of successive irradiations). Such model should support the development of applications, for example it could allow to estimate the effect of laser power stability, which is known to be critical in such applications, on the laser ablation. As short pulse of 100 μs has a minimal heat affected zone, ablation with multiple 100 μs pulses is interesting for applications that require to remove precisely a certain amount of material with minimal heat affected zone. Moreover the linear evolution of depth with

the number of pulses that was evidenced in our work is of interest to calculate the required spatial distribution of irradiations to achieve complex structures.

DATA AVAILABILITY STATEMENT

The data that support the findings of this study are available from the corresponding author upon reasonable request.

Appendix A: Appendix: thermal and optical properties of silica used in this work

- Real part of refractive index: $n_r = 2.4$
- Imaginary part of refractive index: $n_i = 4.628 \times 10^{-2} + 1.01 \times 10^{-4} \times T$
- Emissivity: $\epsilon = 0.8$
- Density: $\rho = 2500\, kg/m^3$
- Evaporation temperature: $T_v = 3085\, K$
- Evaporation enthalpy: $U = 475\, kJ/mol$
- Molar mass: $= 40 \times 10^{-3}\, kg/mol$
- Specific heat: $C_p = -119.6 + 4.5623 \times T - 7.3779 \times 10^{-3} \times T^2 + 6.5913 \times 10^{-6} \times T^3 - 3.0554 \times 10^{-9} \times T^4 + 5.7158 \times 10^{-13} \times T^5$ J/kg/K for $300\, K < T < 1500\, K$; $678.25 - 0.14232 \times T + 3.451 \times 10^{-4} \times T^2$ J/kg/K for $1500\, K < T < 1696\, K$; 1429 J/kg/K for $T > 1696\, K$
- Thermal conductivity: $K = 1.43183 \times 10^{-3} \times T + 0.92885$ W/m/K for $300\, K < T < 1400\, K$; $K = -1.9029 \times 10^{-3} \times T + 5.56413$ W/m/K for $1400\, K < T < 1872 K$; 2 W/m/K for $T < 1872\, K$
- Initial fictive temperature: $T_f = 1413\, K$
- Evaporation coefficient: $\beta = 0.0145$
- Relaxation time: $\tau_0 = 1.064 \times 10^{-17}$ s

REFERENCES

[1]C. Weingarten, A. Schmickler, E. Willenborg, K. Wissenbach, and R. Poprawe, "Laser polishing and laser shape correction of optical glass," Journal of Laser Applications **29**, 011702 (2017).

[2]S. Schwarz, S. Rung, C. Esen, and R. Hellmann, "Fabrication of a high-quality axicon by femtosecond laser ablation and co_2 laser polishing for quasi-bessel beam generation," Optics Express **26**, 23287 (2018).

[3]L. Zhao, J. Cheng, M. Chen, X. Yuan, W. Liao, Q. Liu, H. Yang, and H. Wang, "Formation mechanism of a smooth, defect-free surface of fused silica optics using rapid CO 2 laser polishing," International Journal of Extreme Manufacturing **1**, 035001 (2019).

[4]Z. Cao, C. Wei, X. Cheng, Y. Zhao, X. Peng, Z. Jiang, and J. Shao, "Ground fused silica processed by combined chemical etching and co2 laser polishing with super-smooth surface and high damage resistance," Optics Letters **45**, 6014–6017 (2020).

[5]C. Kim, I. Sohn, Y. Lee, C. Byeon, S. Kim, H. Park, and H. Lee, "Fabrication of a fused silica based mold for the microlenticular lens array using a femtosecond laser and a co_2 laser," Optical Materials Express **4**, 2233 (2014).

[6]K. Wlodarczyk, N. Weston, M. Ardron, and D. Hand, "Direct co_2 laser-based generation of holographic structures on the surface of glass," Optics Express **24**, 1447 (2016).

[7]K. Ott, S. Garcia, R. Kohlhaas, K. Schüppert, P. Rosenbusch, R. Long, and J. Reichel, "Millimeter-long fiber fabry-perot cavities," Optics Express **24**, 9839–9853 (2016).

[8]C. Zhang, W. Liao, K. Yang, T. Liu, Y. Bai, L. Zhang, X. Jiang, J. Chen, Y. Jiang, H. Wang, X. Luan, H. Zhou, X. Yuan, and W. Zheng, "Fabrication of concave microlens arrays by local fictive temperature modification of fused silica," Optics Letters **42**, 1093 (2017).

[9]M. Lai, K. Lim, D. Gunawardena, H. Yang, W. Chong, and H. Ahmad, "Thermal stress modification in regenerated fiber bragg grating via manipulation of glass transition temperature based on co_2-laser annealing," Optics Letters **40**, 748 (2015).

[10]K. Boyd, N. Simakov, A. Hemming, J. Daniel, J. Swain, E. Mies, S. Rees, W. Clarkson, and J. Haus, "Co_2 laser-fabricated cladding light strippers for high-power fiber lasers and amplifiers," Applied Optics **55** (2016).

[11]E. Uzcengiz Simsek, B. Simsek, and B. Ortaç, "Co_2 laser polishing of conical shaped

optical fiber deflectors," Applied Physics B **123**, 176 (2017).

[12]H. Nguyen, M. M. P. Arnob, A. T. Becker, J. C. Wolfe, M. K. Hogan, P. J. Horner, and W.-C. Shih, "Fabrication of multipoint side-firing optical fiber by laser micro-ablation," Optics Letters **42**, 1808–1811 (2017).

[13]S. Fan and N. Healy, "Co2 laser-based side-polishing of silica optical fibers," Optics Letters **45**, 4128–4131 (2020).

[14]M. Matthews, S. Yang, N. Shen, S. Elhadj, R. Raman, G. Guss, I. Bass, M. Nostrand, and P. Wegner, "Micro-shaping, polishing, and damage repair of fused silica surfaces using focused infrared laser beams," Advanced Engineering Materials **17**, 247 (2015).

[15]P. Cormont, A. Bourgeade, S. Cavaro, T. Donval, T. Doualle, G. Gaborit, L. Gallais, L. Lamaignère, and J.-L. Rullier, "Relevance of carbon dioxide laser to remove scratches on large fused silica polished optics," Advanced Engineering Materials **17**, 253 (2015).

[16]T. Doualle, L. Gallais, S. Monneret, S. Bouillet, A. Bourgeade, C. Ameil, L. Lamaignère, and P. Cormont, "Co_2 laser microprocessing for laser damage growth mitigation of fused silica optics," Optical Engineering **56**, 011022 (2017).

[17]C. Tan, L. Zhao, M. Chen, J. Cheng, C. Wu, Q. Liu, H. Yang, Z. Yin, and W. Liao, "Experimental and theoretical investigation of localized co2 laser interaction with fused silica during the process of surface damage mitigation," Results in Physics **16**, 102936 (2020).

[18]C. Zhang, L. Zhang, X. Jiang, B. Jia, W. Liao, R. Dai, J. Chen, X. Yuan, and X. Jiang, "Influence of pulse length on heat affected zones of evaporatively-mitigated damages of fused silica optics by co2 laser," Optics and Lasers in Engineering **125**, 105857 (2020).

[19]Y. Xiao and M. Bass, "Thermal stress limitations to laser fire polishing of glasses," Applied Optics **22**, 2933 (1983).

[20]G. Allcock, D. Dyer, G. Elliner, and H. Snelling, "Experimental observations and analysis of co_2 laser-induced microcracking of glass," Journal of Applied Physics **78**, 7295 (1995).

[21]M. Feit, A. Rubenchik, C. Boley, and M. Rotter, "Development of a process model for co_2 laser mitigation of damage growth in fused silica," Proc. SPIE **5273**, 145–154 (2004).

[22]K. Nowak, H. Baker, and Hall, "Analytical model for co_2 laser ablation of fused quartz," Applied Optics **54**, 8653 (2015).

[23]R. Vignes, T. Soules, J. Stolken, R. Settgast, S. Elhadj, and M. Matthews, "Thermomechanical modeling of laser-induced structural relaxation and deformation of glass: Volume

changes in fused silica at high temperatures," Journal of the American ceramic Society **96**, 137–145 (2013).

[24]T. Doualle, L. Gallais, P. Cormont, Hebert, P. Combis, and J.-L. Rullier, "Thermomechanical simulations of co_2 laser–fused silica interactions," Journal of Applied Physics **119**, 113106 (2016).

[25]L. Robin, P. Combis, P. Cormont, L. Gallais, D. Hebert, C. Mainfray, and J. L. Rullier, "Infrared thermometry and interferential microscopy for analysis of crater formation at the surface of fused silica under co_2 laser irradiation," Journal of Applied Physics **111**, 063106 (2012).

[26]T. Doualle, L. Gallais, P. Cormont, T. Donval, L. Lamaignère, and J. L. Rullier, "Effect of annealing on the laser induced damage of polished and co_2 laser-processed fused silica surfaces," Journal of Applied Physics **119**, 213106 (2016).

[27]T. Doualle, A. ollé, P. Cormont, S. Monneret, and L. Gallais, "Laser-induced birefringence measurements by quantitative polarized-phase microscopy," Optics Letters **42**, 1616 (2017).

[28]A. D. McLachlan and F. P. Meyer, "Temperature dependence of the extinction coefficient of fused silica for co_2 laser wavelengths," Applied Optics **26**, 1728 (1987).

[29]P. Combis, P. Cormont, L. Gallais, D. Hebert, L. Robin, and J.-L. Rullier, "Evaluation of the fused silica thermal conductivity by comparing infrared thermometry measurements with two-dimensional simulations," Applied Physics Letters **101**, 211908 (2012).

[30]T. D. Bennett, D. J. Krajnovich, and L. Li, "Thermophysical modeling of bump formation during co 2 laser texturing of silicate glasses," Journal of Applied Physics **85**, 153 (1999).

[31]T. D. Bennett, D. J. Krajnovich, L. Li, and D. Wan, "Mechanism of topography formation during co2 laser texturing of silicate glasses," Journal of Applied Physics **84**, 2897–2905 (1998), https://doi.org/10.1063/1.368396.

[32]M. Tomozawa, A. Koike, and S.-R. Ryu, "Exponential structural relaxation of a high purity silica glass," Journal of non-crystalline solids **354**, 4685 (2008).

[33]T. Doualle, L. Gallais, P. Cormont, T. Donval, L. Lamaignere, and J. Rullier, "Effect of annealing on the laser induced damage of polished and co2 laser-processed fused silica surfaces," Journal of Applied Physics **119**, 213106 (2016).

[34]J. Shelby, "Density of vitreous silica," Journal of Non Crystalline-Solids **349**, 331 (2016).

[35]M. D. Feit, M. J. Matthews, T. F. Soules, J. S. Stolken, R. M. Vignes, S. T. Yang, and

J. D. Cooke, "Densification and residual stress induced by CO2 laser-based mitigation of SiO2 surfaces," in *Laser-Induced Damage in Optical Materials: 2010*, Vol. 7842, edited by G. J. Exarhos, V. E. Gruzdev, J. A. Menapace, D. Ristau, and M. J. Soileau, International Society for Optics and Photonics (SPIE, 2010) pp. 189 – 193.

[36]C. Weingarten, A. Schmickler, E. Willenborg, K. Wissenbach, and R. Poprawe, "Laser polishing and laser shape correction of optical glass," Journal of Laser Applications **29**, 011702 (2017), https://doi.org/10.2351/1.4974905.

[37]E. Mendez, K. M. Nowak, H. J. Baker, F. J. Villarreal, and D. R. Hall, "Localized co_2 laser damage repair of fused silica optics," Applied Optics **45**, 5358–5367 (2006).

[38]S. Elhadj, M. Matthews, G. Guss, and I. Bass, "Laser-based dynamic evaporation and surface shaping of fused silica with assist gases: a path to rimless laser machining," Applied Physics B **113**, 307 (2013).

[39]L. Robin, P. Combis, P. Cormont, L. Gallais, D. Hebert, C. Mainfray, and J.-L. Rullier, "Infrared thermometry and interferential microscopy for analysis of crater formation at the surface of fused silica under co2 laser irradiation," Journal of Applied Physics **111**, 063106 (2012), https://doi.org/10.1063/1.3695375.

[40]H. L. Schick, "A thermodynamic analysis of the high-temperature vaporization properties of silica." Chemical Reviews **60**, 331–362 (1960), https://doi.org/10.1021/cr60206a002.

[41]S. Elhadj, M. J. Matthews, S. T. Yang, and D. J. Cooke, "Evaporation kinetics of laser heated silica in reactive and inert gases based on near-equilibrium dynamics," Optics Express **20**, 1575–1587 (2012).

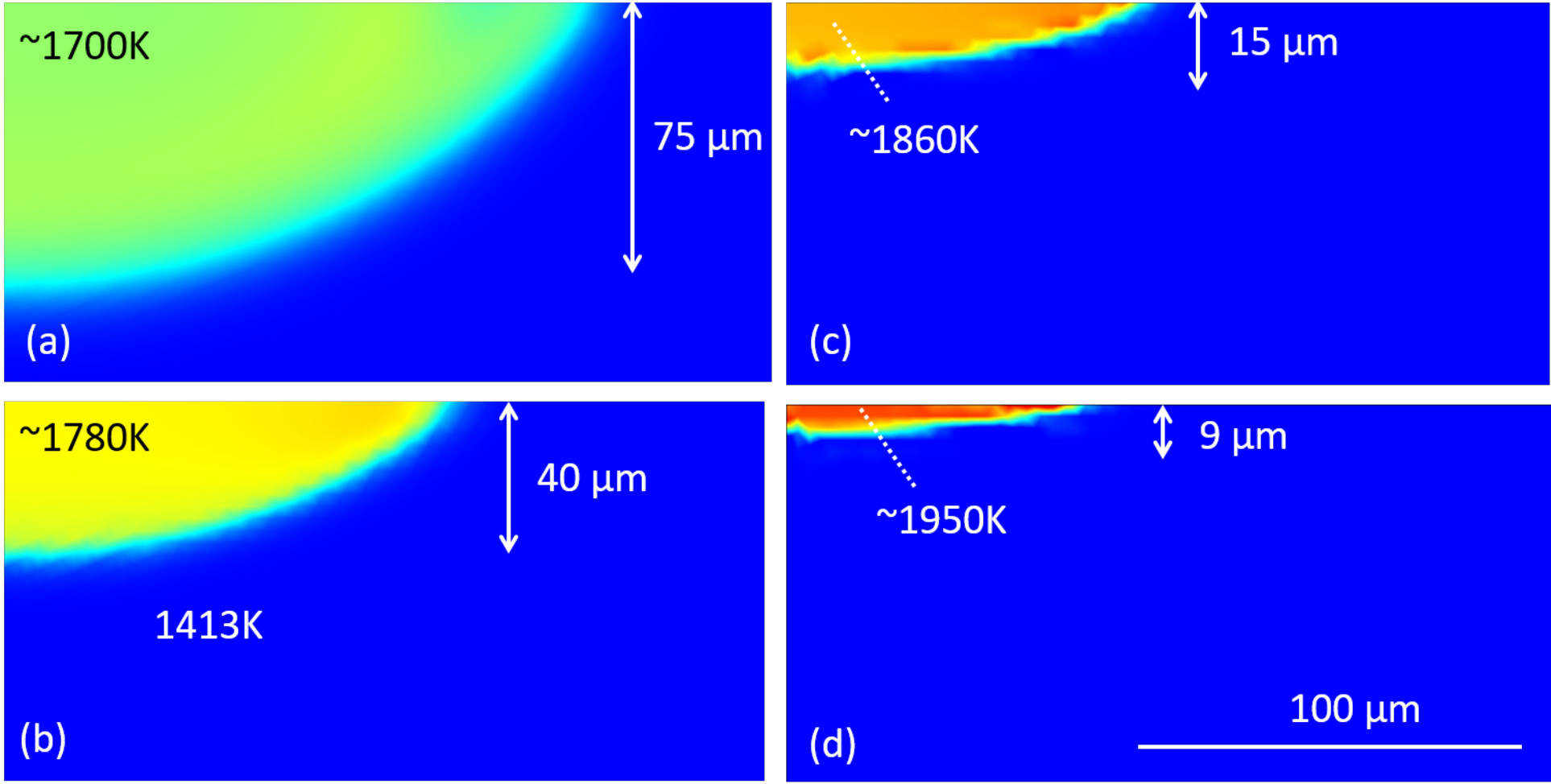
~1700K
75 µm
(a)
~1780K
40 µm
1413K
(b)
15 µm
~1860K
(c)
9 µm
~1950K
100 µm
(d)

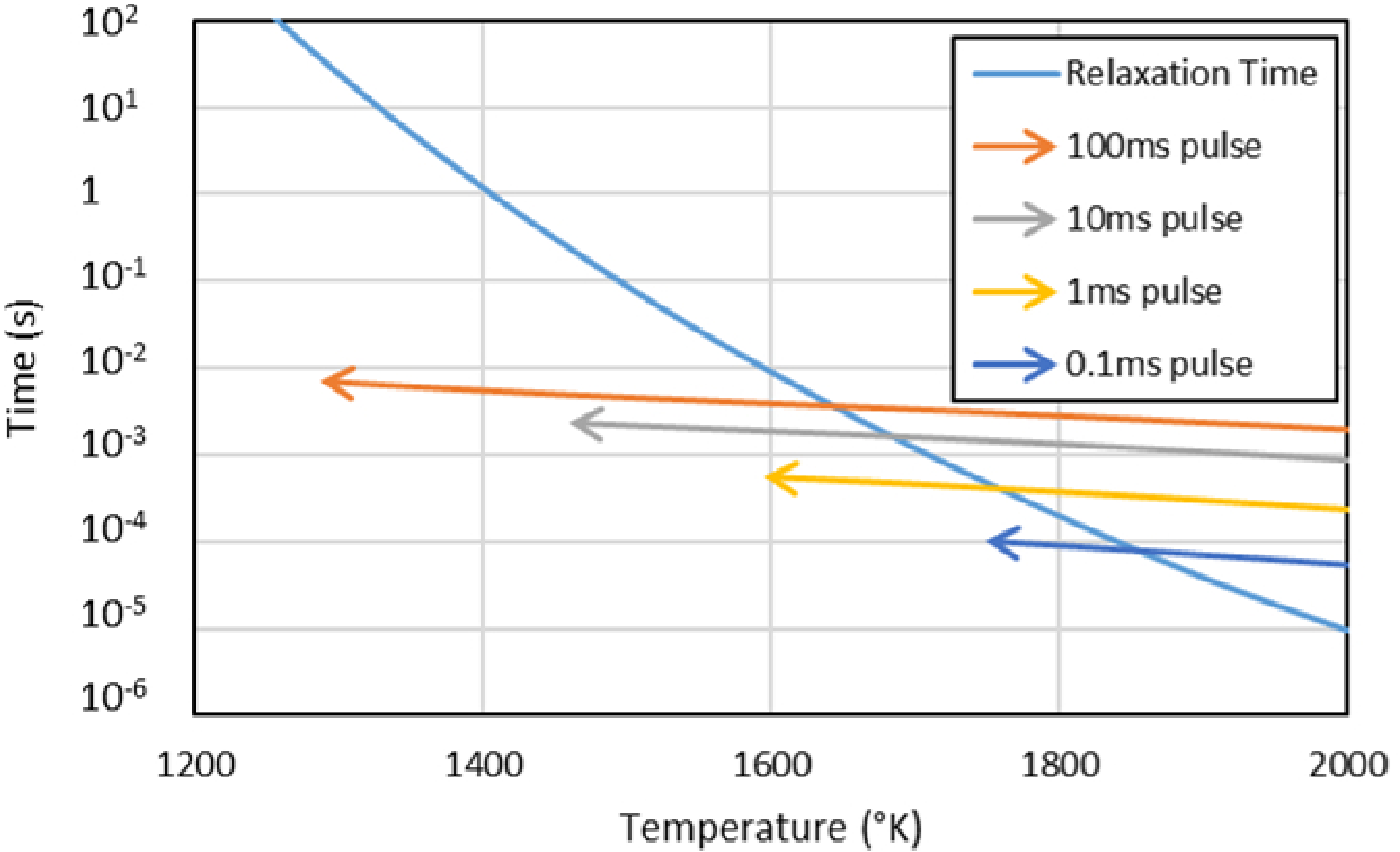
Relaxation Time
100ms pulse
10ms pulse
1ms pulse
0.1ms pulse
Time (s)
10^2
10^1
1
10^-1
10^-2
10^-3
10^-4
10^-5
10^-6
1200
1400
1600
1800
2000
Temperature (°K)

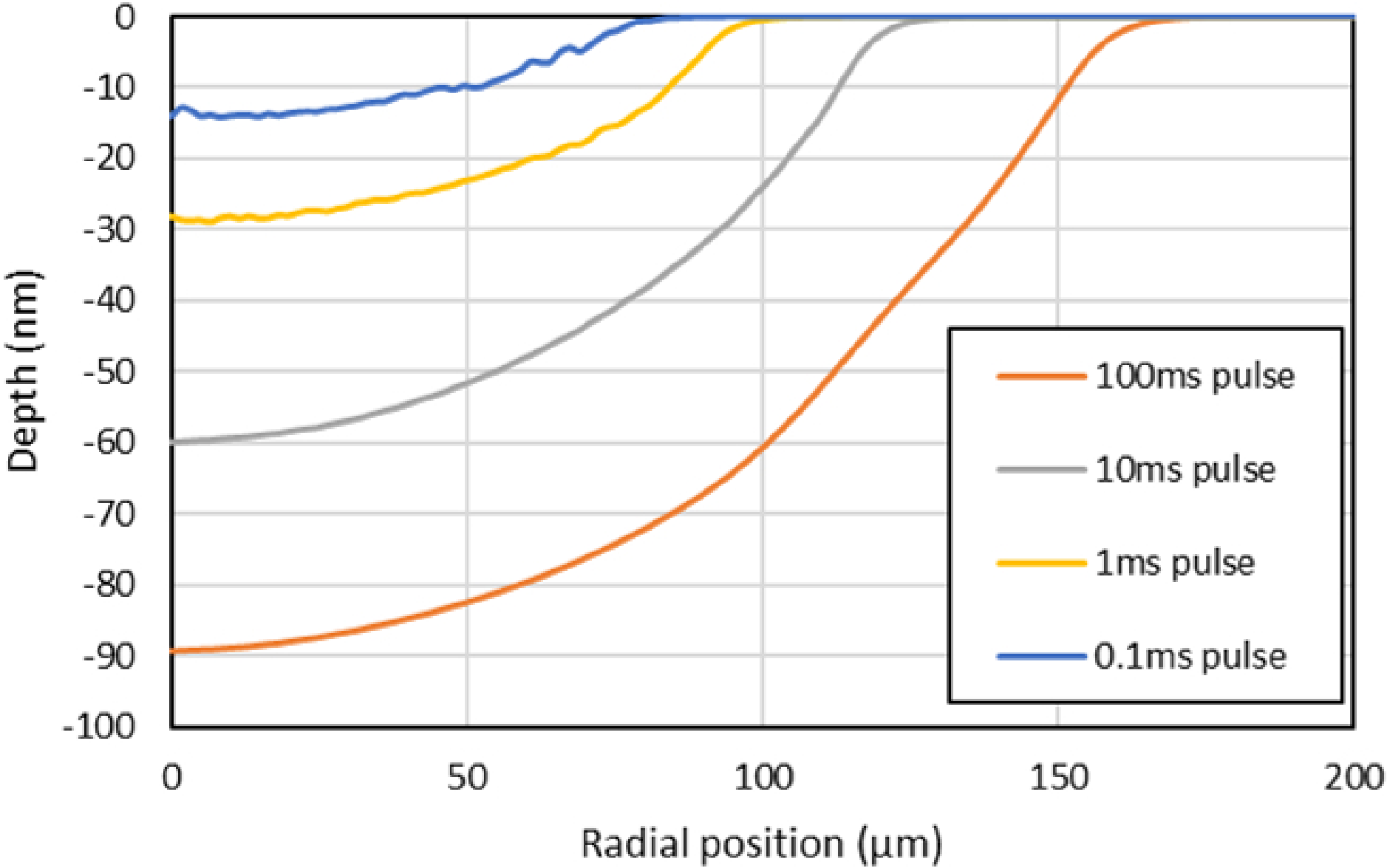
0
-10
-20
-30
-40
-50
-60
-70
-80
-90
-100
Depth (nm)
0
50
100
150
200
Radial position (µm)
100ms pulse
10ms pulse
1ms pulse
0.1ms pulse

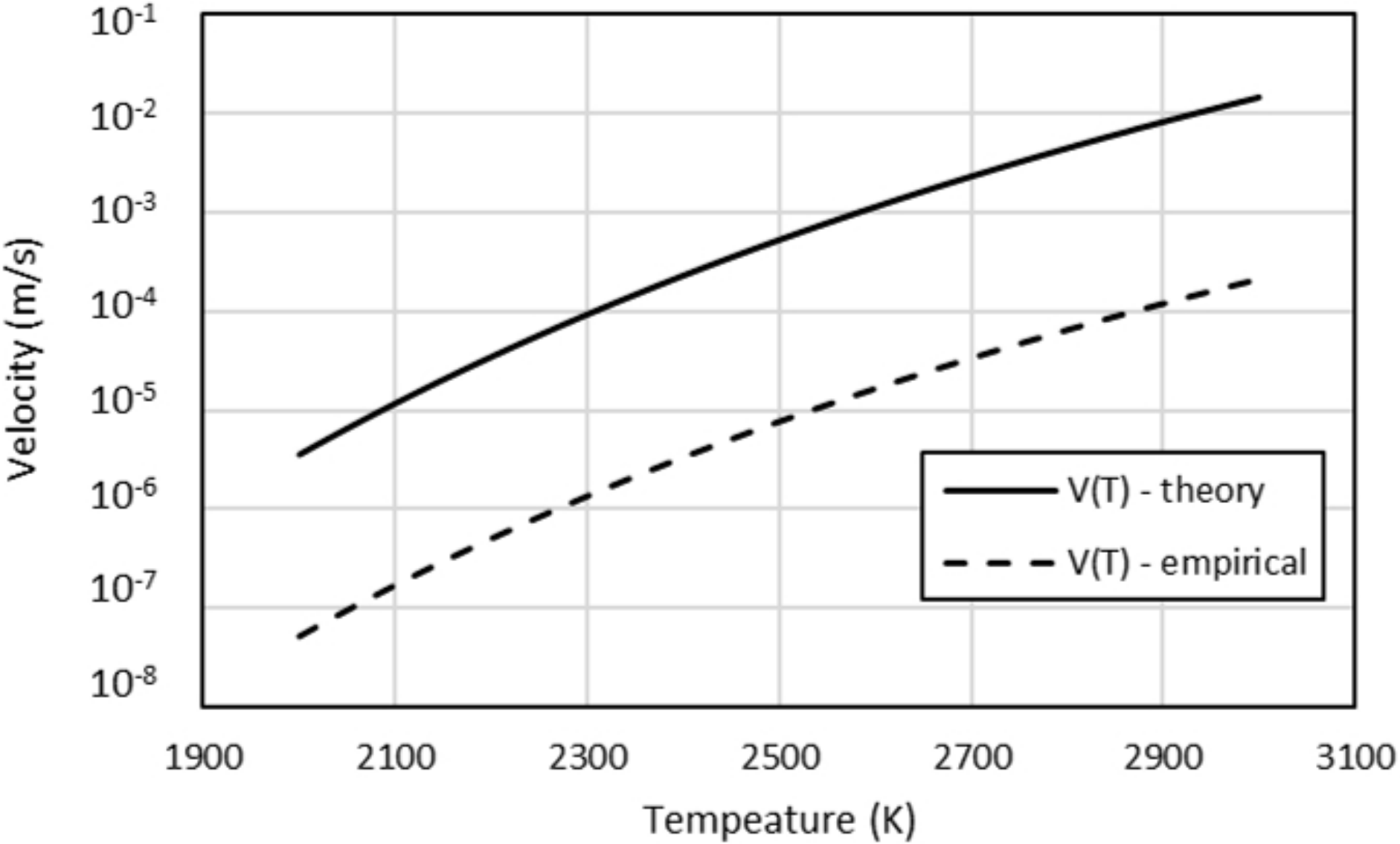
Velocity (m/s)
10-1
10-2
10-3
10-4
10-5
10-6
10-7
10-8
1900
2100
2300
2500
2700
2900
3100
Tempeature (K)
V(T) - theory
V(T) - empirical

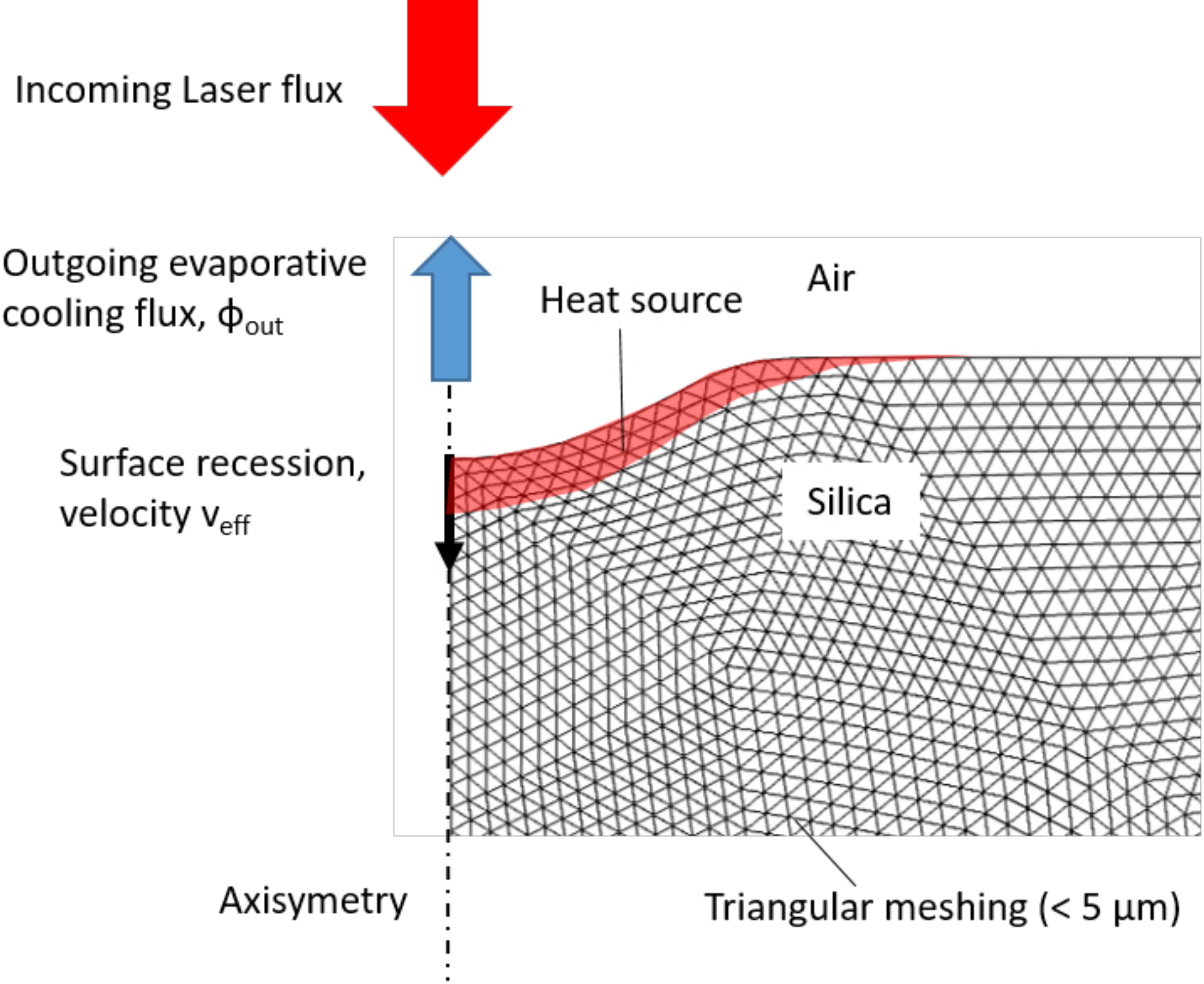
Incoming Laser flux
Outgoing evaporative cooling flux, ϕ_{out}
Surface recession, velocity v_{eff}
Heat source
Air
Silica
Axisymetry
Triangular meshing (< 5 µm)

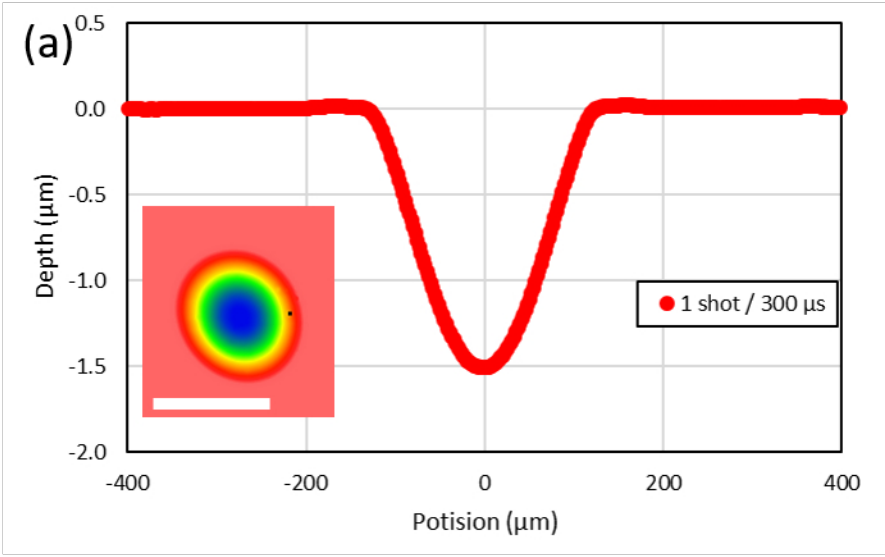
(a)
0.5
0.0
-0.5
-1.0
-1.5
-2.0
Depth (μm)
-400
-200
0
200
400
Potision (μm)
1 shot / 300 μs

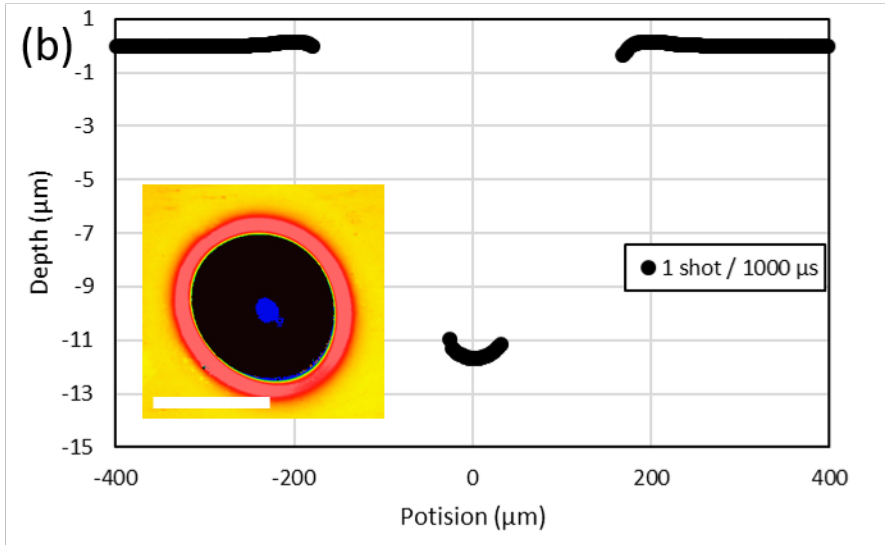
(b)
1
-1
-3
-5
-7
-9
-11
-13
-15
Depth (μm)
-400
-200
0
200
400
Potision (μm)
1 shot / 1000 μs

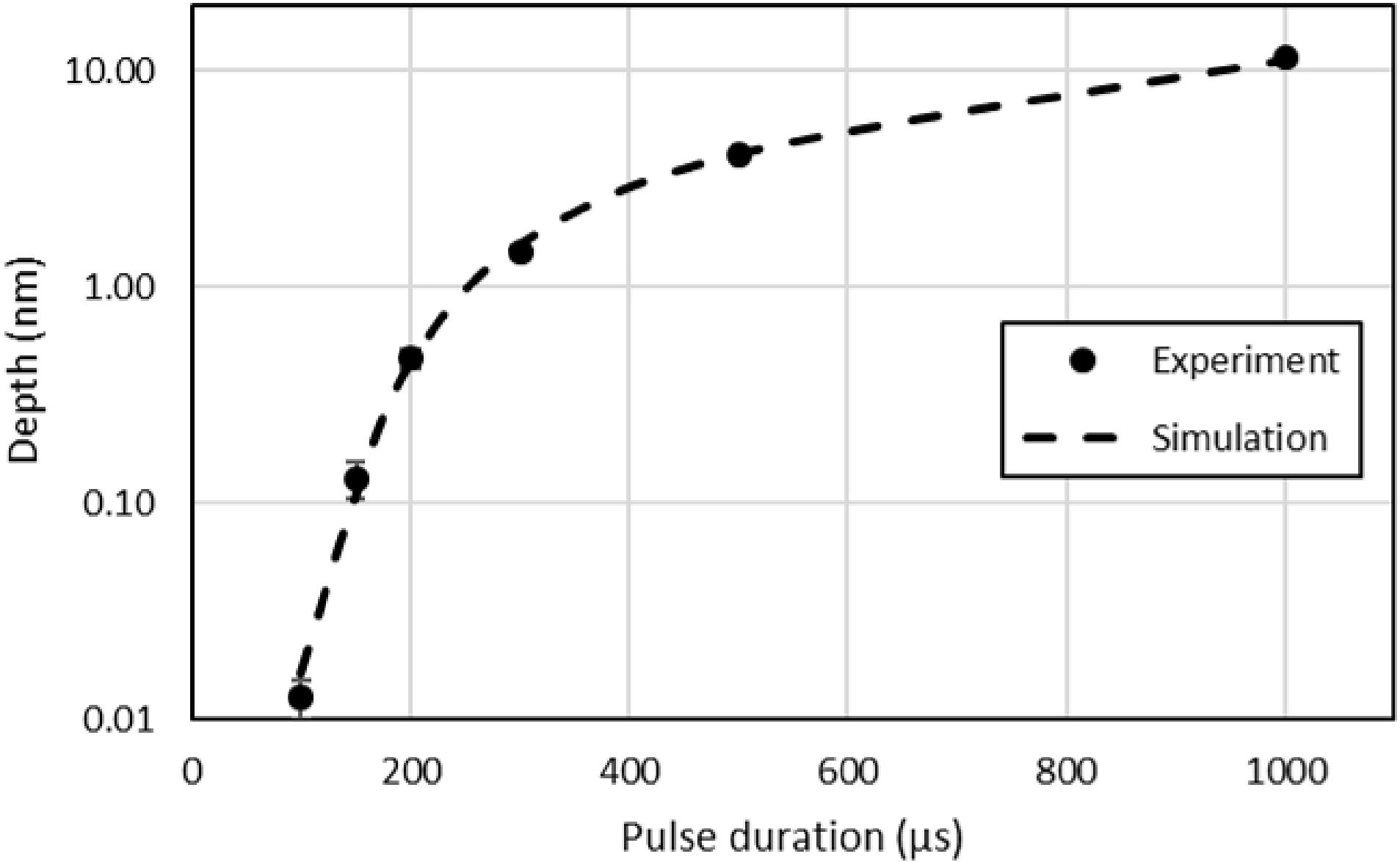
10.00
1.00
0.10
0.01
Depth (nm)
0
200
400
600
800
1000
Pulse duration (µs)
Experiment
Simulation

(a)

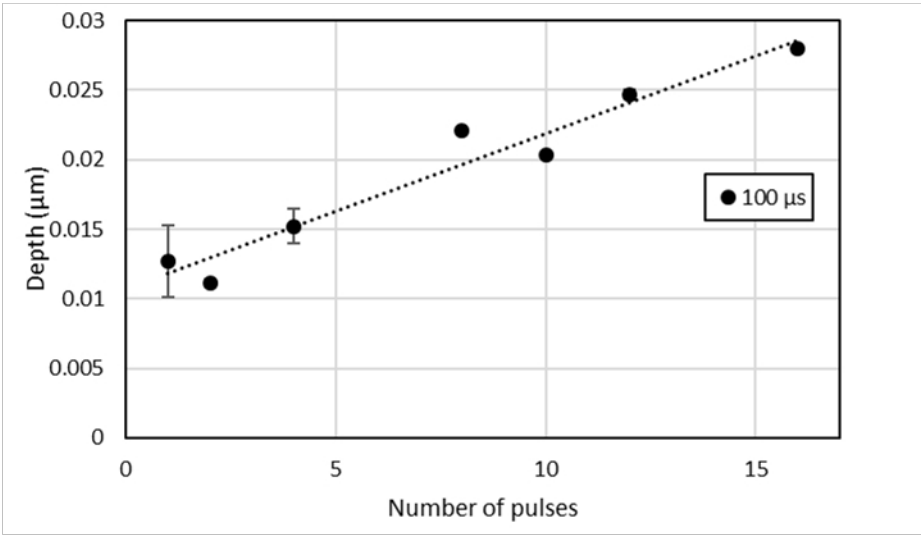
0.03
0.025
0.02
0.015
0.01
0.005
0
Depth (µm)
100 µs
0
5
10
15
Number of pulses

(b)

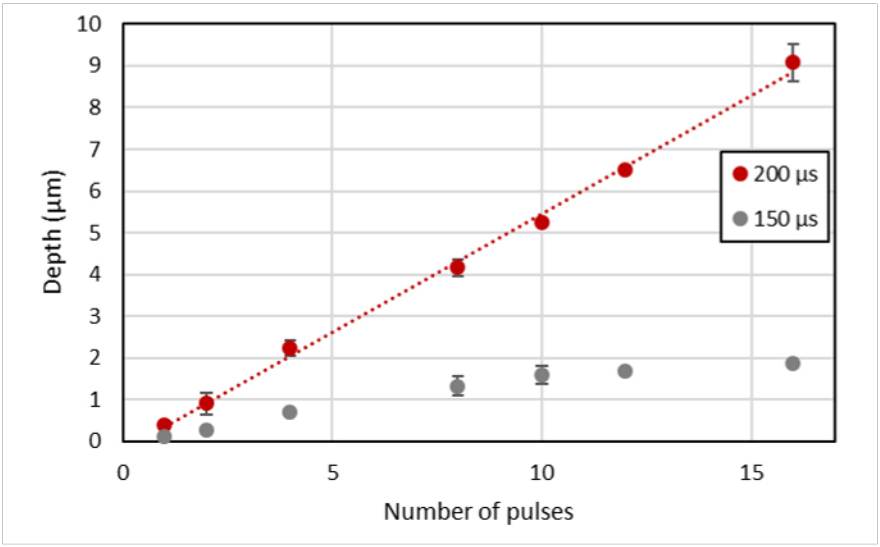
10
9
8
7
6
5
4
3
2
1
0
Depth (µm)
200 µs
150 µs
0
5
10
15
Number of pulses

(c)

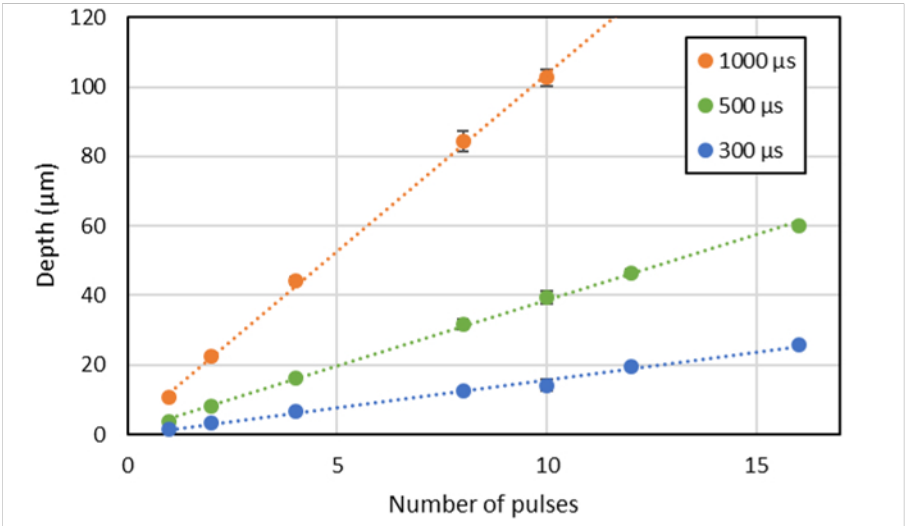
120
100
80
60
40
20
0
Depth (µm)
1000 µs
500 µs
300 µs
0
5
10
15
Number of pulses

(a)

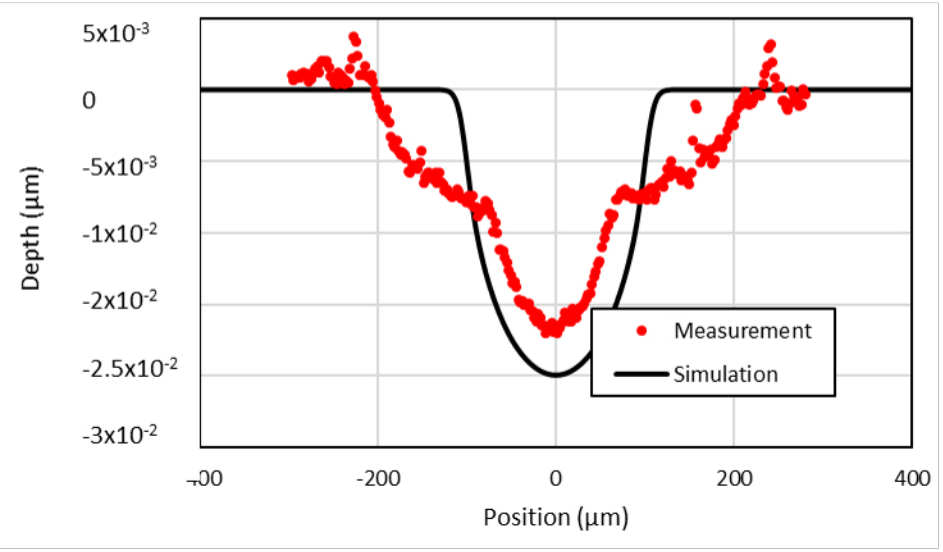
5x10-3
0
-5x10-3
-1x10-2
-2x10-2
-2.5x10-2
-3x10-2
Depth (µm)
-400
-200
0
200
400
Position (µm)
Measurement
Simulation

(b)

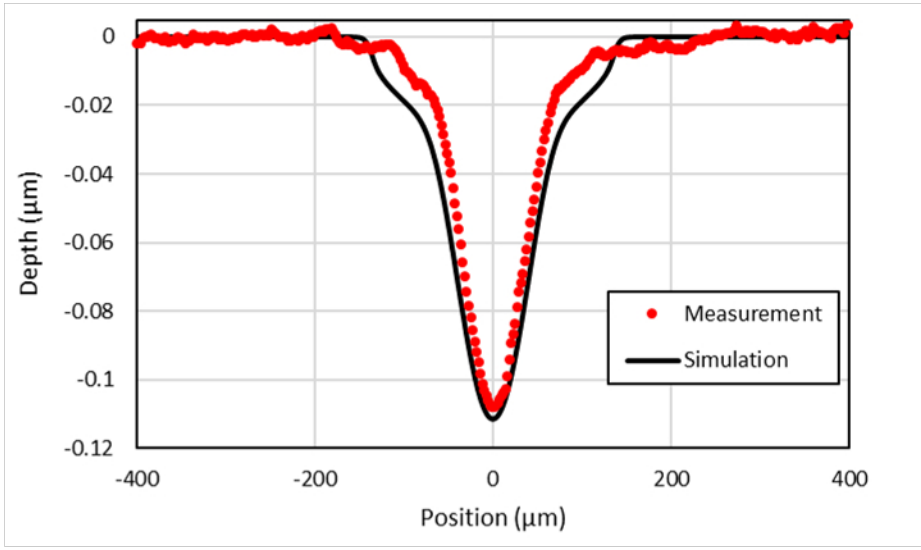
0
-0.02
-0.04
-0.06
-0.08
-0.1
-0.12
Depth (µm)
-400
-200
0
200
400
Position (µm)
Measurement
Simulation

(c)

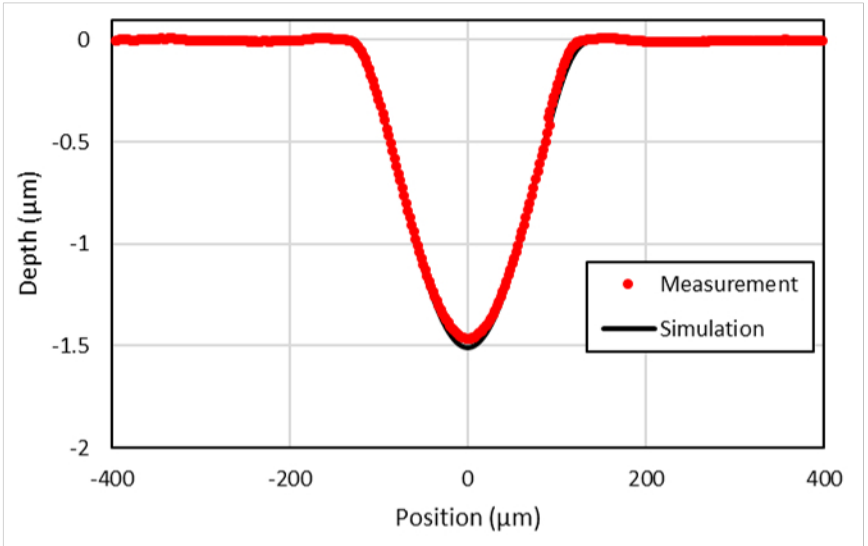
0
-0.5
-1
-1.5
-2
Depth (µm)
-400
-200
0
200
400
Position (µm)
Measurement
Simulation

(d)

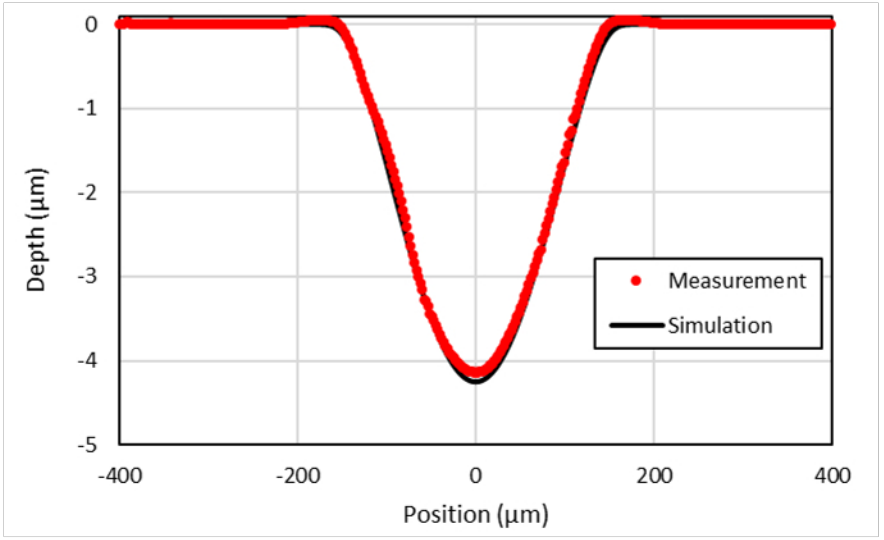
0
-1
-2
-3
-4
-5
Depth (µm)
-400
-200
0
200
400
Position (µm)
Measurement
Simulation

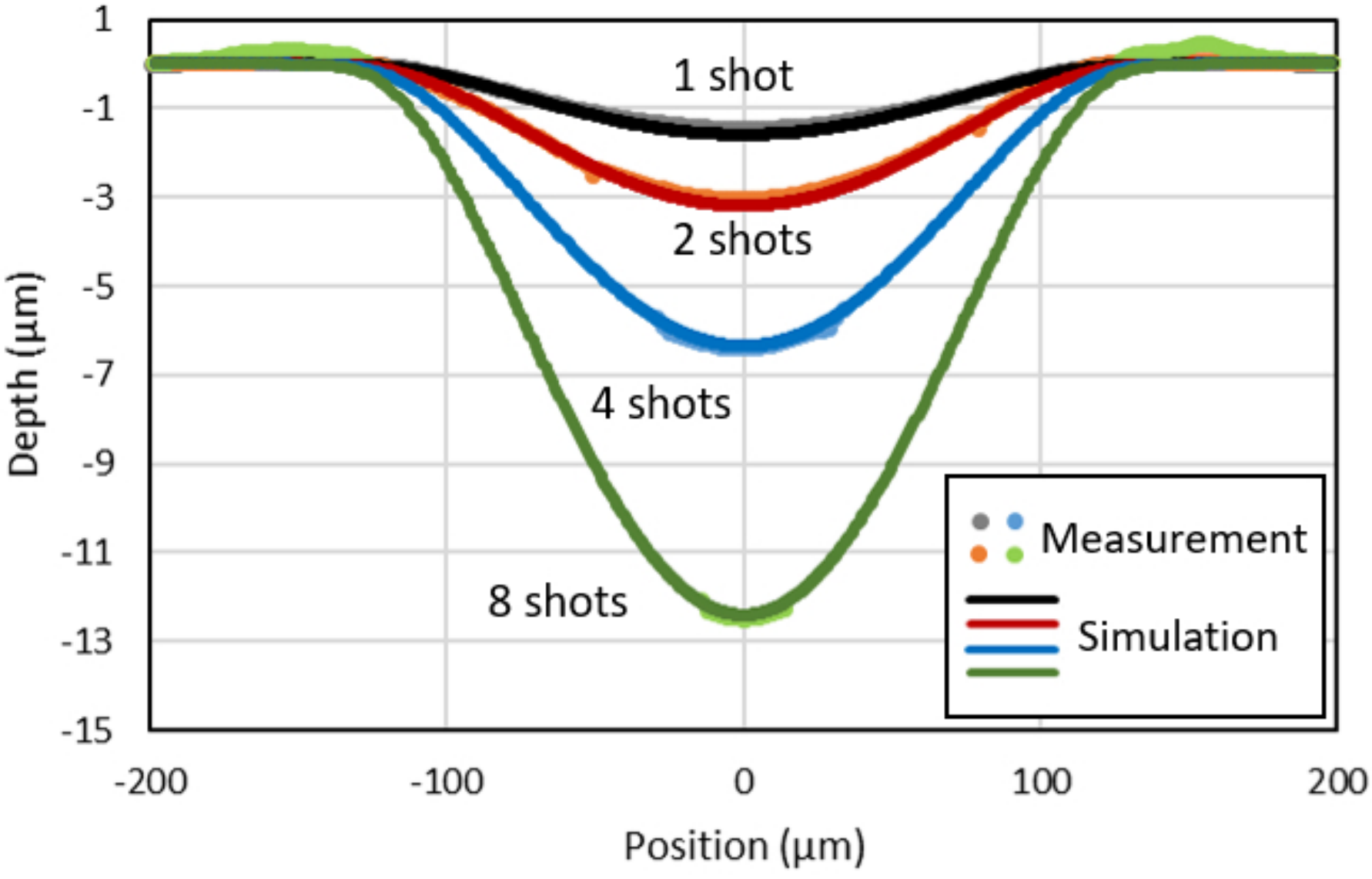
1
-1
-3
-5
-7
-9
-11
-13
-15
Depth (µm)
1 shot
2 shots
4 shots
8 shots
Measurement
Simulation
-200
-100
0
100
200
Position (µm)